Available online at www.sciencedirect.com
ScienceDirect
ELSEVIER
International Journal of Rock Mechanics & Mining Sciences 45 (2008) 1126–1142
International Journal of Rock Mechanics and Mining Sciences
www.elsevier.com/locate/ijrmms

Numerical modelling of uniaxial compressive failure of granite with and without saline porewater

Ann Bäckström[a,*], Juha Antikainen[b], Tobias Backers[c], Xiating Feng[d], Lanru Jing[e], Akira Kobayashi[f], Tomofumi Koyama[e], Pengzhi Pan[d], Mikael Rinne[g], Baotang Shen[g], John A. Hudson[h]

[a]*Royal Institute of Technology, Stockholm, Sweden, and Berg Bygg Konsult AB, Ankdammsgatan 20, 17143 Solna, Stockholm, Sweden*
[b]*Helsinki University of Technology, Finland*
[c]*GeoFrames GmbH, Germany*
[d]*State Key Laboratory of Geomechanics and Geotechnical Engineering, Institute of Rock and Soil Mechanics, Chinese Academy of Sciences, China*
[e]*Royal Institute of Technology, Stockholm, Sweden*
[f]*Kyoto University, Japan*
[g]*Fracom Ltd., Finland*
[h]*Rock Engineering Consultants and Imperial College, UK*

Received 13 March 2007; received in revised form 26 November 2007; accepted 2 December 2007
Available online 28 January 2008

Abstract

It is important for rock engineering design to be able to validate numerical simulations, i.e. to check that they adequately represent the rock reality. In this paper, the capability and validity of four numerical models is assessed through the simulation of an apparently simple case: the complete process of microstructural breakdown during the uniaxial compressive failure of intact crystalline rock. In addition to comparing the capabilities of the four models, the results generated by each model were compared with the experimentally determined complete stress–strain curves for the Swedish Ävrö granite for different porewater conditions. In this way, it has been possible to audit the models' adequacy for this particular simulation task. It was found that although the models had common features, they were each idiosyncratically different and required considerable expertise to match the actual stress–strain curves (which did not monotonically increase in axial strain)—indicating that, for more complex simulations, both adequate modelling and appropriate validation are not going to be an easy task. The work was conducted within the framework of the international 2004–2007 DEmonstration of COupled models and their VALidation against EXperiments with emphasis on Thermo Hydro Mechanic and Chemical aspects (DECOVALEX-THMC) phase on coupled modelling extended to include chemical effects and with application to the excavation damaged zone (EDZ) in crystalline rock.

Keywords: Numerical modelling; Uniaxial compressive strength; Class II behaviour; Chemical degradation; Auditing process; Crystalline rock; DECOVALEX-THMC

1. Introduction

1.1. Numerical modelling versus reality and the purpose of this paper

The rock engineer designing a structure to be supported by or contained within a rock mass must have a predictive ability in order to be able to estimate the likely consequences of constructing the structure to any particular design; this predictive capability is usually provided by some form of model. Over recent decades, numerical models have gradually replaced the use of analytical solutions and physical models as the main support for rock engineering design. Numerical models have many advantages, including the current ability to incorporate all the idiosyncratic discontinuous, inhomogeneous, anisotropic and non-elastic (DIANE) features of real rock

*Corresponding author. Tel.: +4687595050; fax: +4687595065.
E-mail address: ann.backstrom@bergbyggkonsult.se (A. Bäckström).

1365-1609/$ - see front matter © 2008 Elsevier Ltd. All rights reserved.
doi:10.1016/j.ijrmms.2007.12.001

masses [1] and to provide solutions and associated sensitivity analyses quickly and reliably. However, despite the rapid growth of these numerical modelling capabilities, there has been no commensurate growth in methods of checking the consistency, validity and appropriateness of the numerical modelling methods and solutions, i.e. no internationally recognized auditing process is available to ensure that the modelling does indeed represent the rock reality.

The objective of this paper is to report on a programme of work in which the most fundamental mechanical behaviour of rock, the structural collapse of a granite rock sample in uniaxial compression, was studied both experimentally in the laboratory and via four different numerical modelling approaches. The emphasis was put on the reproduction of the Class II behaviour of the rock type, Ävrö granite, used in these experiments. The Ävrö granite from the Äspö Hard Rock Laboratory in Sweden is extremely brittle—which provided an extra challenge for both laboratory experiment and numerical modelling. The numerical modelling results from four different modelling groups using different approaches were compared with each other and with the laboratory test results. Note that the four approaches were pre-defined because they were part of the DEmonstration of COupled models and their VALidation against EXperiments with emphasis on Thermo Hydro Mechanic and Chemical aspects (DECOVALEX-THMC) [2].

In this way, the common and special features of the different modelling techniques could be established, together with an assessment of the advantages and disadvantages of the different modelling techniques, plus the validity of the modelling techniques. This approach to the validation subject was used because it is appropriate to begin with the most basic mechanical behaviour. Wawersik [3] recommended that to limit the complexity of the system initially employed for the validation of modelling, laboratory scale tests are recommended. Although it must be born in mind that when it comes to natural material like rock the microscopic inhomogeneities in the material increase the variation of the laboratory test results and predictions of the behaviour of the material are compromised compared to investigation on man-made materials.

1.2. The uniaxial compression test and the complete stress–strain curve

Accordingly, this paper reports on the results of an exercise to model the uniaxial compressive failure of intact rock with and without saline porewater using different numerical models and to assess the results both through inter-comparison of the results from the different models and by direct comparison with experimental results.

In his pioneering work and using a stiff testing machine, Wawersik [4] obtained a series of complete stress–strain curves for different rock types (Fig. 1). The complete curve is important because in some rock engineering applications, and as opposed to the design of conventional civil engineering buildings, parts of the rock mass can have entered the failure region due to the stress situation and accumulated damage, i.e. the stress–strain region beyond the peak stress. It is necessary to understand this stress–strain behaviour before and after the peak stress and subsequently test the hypothesis by reproducing it with a model for a complete understanding of rock failure.

Moreover, Wawersik identified two fundamental modes of stress–strain behaviour in uniaxial compression: Class I and Class II, as illustrated in Fig. 1. A Class I complete

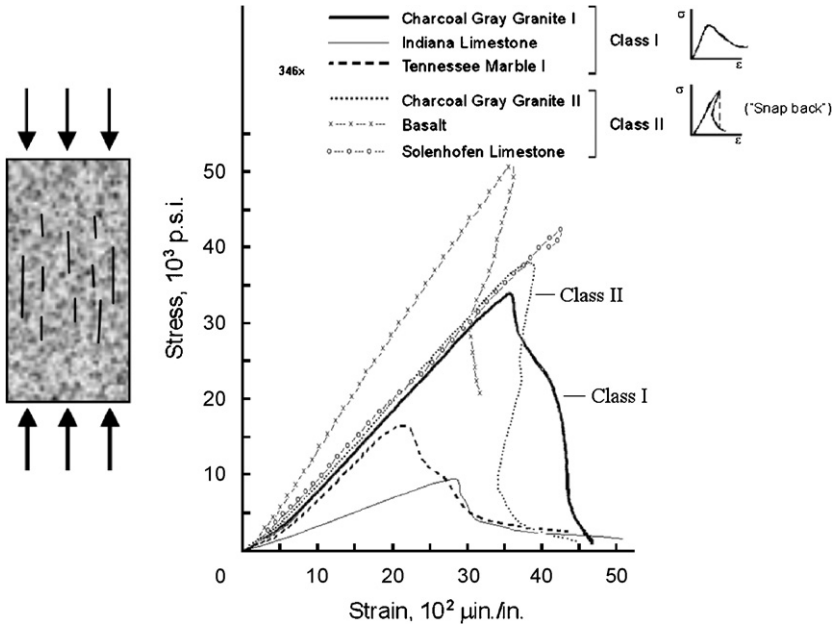

Fig. 1. (a) The uniaxial compression test on rock and (b) complete stress–strain curves obtained in [2], where Class I and Class II behaviour is indicated.

stress–strain curve monotonically increases in axial strain; a Class II complete stress–strain curve does not monotonically increase in axial strain. Note that from the nature of the curves displaying the different behaviour indicated in Fig. 1(b), neither curve can be obtained by programming a linear increase in axial stress (because the curves do not monotonically increase in axial stress) and a Class II curve cannot be obtained by programming a linear increase in axial strain (because the Class II curve does not monotonically increase in axial strain).

The keys to understanding the Class II curve are that (a) the curve represents the structural breakdown of a rock specimen, (b) after the peak, the curve is a locus of the rock failure condition, and (c) at the peak stress and some of the following post-peak stress levels, the rock specimen contains more strain energy than is required to continue the failure process, and so energy has to be withdrawn.

Thus, if a constant stress increase or a constant axial strain increase is programmed for the test when the rock behaviour is Class II, the result will be uncontrolled collapse. To be able to describe the Class II post-peak behaviour energy must be extracted from the rock to prevent its violent collapse [5]. For example, in the lateral strain control situation, the lateral displacement monotonically increases but the axial displacement reverses, so programming the rate of the lateral strain as the control mode prevents abrupt failure and allows the complete stress–strain curve to be obtained.

1.3. The overall context of the modelling work

Despite the value of numerical simulations and their considerable appeal through their ability to incorporate the rock's DIANE characteristics, the auditing issue should be borne in mind. Rock engineers concerned with whether models correctly simulate the rock reality have to ask questions such as the following. How does one obtain the correct input parameters to model a specific rock type? If different numerical models are used, will the same resulting stress–strain curve be obtained from the different approaches? Can the code model Class II behaviour? Can the numerical model be validated? In other words, is there some method of checking whether the model output is the same as the real rock response?

This paper reports on the results of an exercise to model the uniaxial compressive failure of intact rock with and without saline porewater, using different numerical models and to assess the results both through inter-comparison of the results from the different models and by direct comparison with experimental results. The study reported here was conducted within the context of improving understanding of the evolution of the excavation damage zone (EDZ). Depending on the excavation method the extent of the EDZ will be different [6,7]. Due to the inherent nature of blasting and its incremental progress, this excavation method generally produces a larger EDZ than when a tunnel boring machine is used with its relatively gentler penetration of the rock mass [6,8,9].

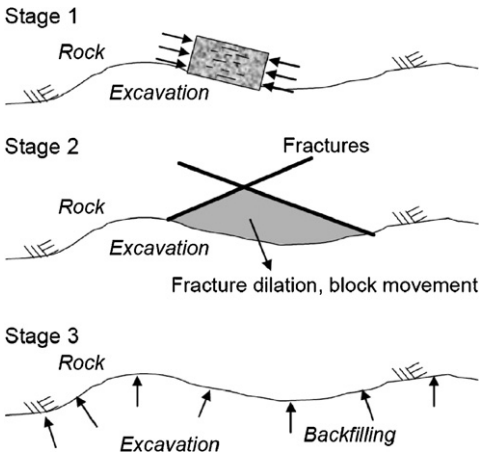

Fig. 2. The different stages of development of the EDZ during the lifetime of the repository.

The development of the EDZ was divided into three stages in the overall study, as shown in Fig. 2. Stage 1 is the initial construction, which alters the mechanical, hydrological and chemical circumstances. Stage 2 is a period when the excavation is left open, when drying of the rock occurs, water flows through the rock fractures, and there can be chemical changes. Stage 3 is the period following the emplacement of the canisters and backfill, after which the temperature increases, and equilibrium is re-established over a long-time period.

The work reported in this paper concerns Stage 1 and the numerical modelling the potential failure of the intact rock induced by the secondary stresses located at the periphery of the excavation. Four different modelling programmes were used by four different modelling groups, and compared to experimental uniaxial compressive tests on granite specimens. Thus, the study concerns the understanding and characterization of the complete failure process of intact rock in uniaxial compression using different numerical models, physical testing with chemical effects and co-ordination of the results. In the experimental tests to obtain the complete stress–strain curve for intact rock samples in uniaxial compression, the influence of the hydro-chemical environment (with emphasis on saline porewater) was also investigated. The capabilities and results of the numerical modelling using different codes are compared to each other and the physical test results in order to evaluate the benefits and drawbacks of the different approaches.

2. Laboratory testing and results for the Ävrö granite

A series of laboratory tests was performed to obtain the complete stress–strain curves and to address the chemical and time-dependent influences on the mechanical strength of a crystalline intact rock. The tests were all conducted on Ävrö granite from the Äspö Hard Rock Laboratory

(ÄHRL) in Sweden. From the modal analysis made on five of the specimens, they are mainly composed of feldspar, quartz and mica in the following percentages, 66%, 25% and 6%, respectively [10].

2.1. Uniaxial compressive test on Ävrö granite

In the first set, uniaxial compression tests were performed for different hydro-chemical influences with different salinity and saturation porewater environments [11]. The 20 specimens were divided into four groups with five specimens in each group. The first group was composed of specimens that had been dried and the rest of the samples were saturated with fluids having different salinities. Group 2 specimens were saturated with distilled water, according to the ISRM Suggested Method [12]; whereas, the specimens in the two last groups were saturated with waters having a salinity of 0.68% (denoted 'formation water') and 10% (denoted 'saline water'). Most of the specimens were saturated for 90 days, but two of the specimens saturated with distilled water and three of the specimens saturated with formation water had a saturation time of only 40 days.

The uniaxial compressive tests were performed using a servo-controlled testing machine having a maximum loading capacity of 1.5 MN. As described in Section 1.2, a special technique was required to obtain the Class II behaviour exhibited by the Ävrö granite and the initial control programme was set to a radial strain rate of 0.025%/min until well beyond the peak strength. This rate was increased to 0.04%/min after about 20 min when the specimen behaviour had reached well into the post-peak region. The tests were carried out to the post-peak regime in order to study the mechanical behaviour of the rock during the cracking process.

From photographs of the Ävrö granite (Fig. 3), taken prior to the compressive test, it can be seen that the specimens in this study have a set of 'sub-lateral' pre-existing cracks.

The pre-existing fracturing shown in Fig. 3(b) (the white lines) has been caused by an earlier stress field. It is unlikely that this pre-existing fracturing has been induced by the coring process—because of the orientational uniformity of the fracturing across the specimen. However, the induced fractures caused by the uniaxial compression testing interact with the pre-existing fractures. In Fig. 4, the completion of the stress–stain curve is shown. When this stage was reached, the sample was sectioned, vacuum impregnated with fluorescent epoxy and photographed to illustrate the fracturing shown in Fig. 5(a).

In the two photographs in Figs. 5(b) and (c), the pre-existing fracturing is represented by the sub-lateral cracks and the fracturing induced by testing is represented by the sub-axial cracks—with both types of fracturing occurring in the lighter coloured minerals, the feldspar and quartz. Although there is evidence of some interaction between the two sets of cracks (the pre-existing cracks have acted either as initiators or inhibitors of the induced cracks), no difference in the fracture interaction between the samples with different porewater composition has been identified.

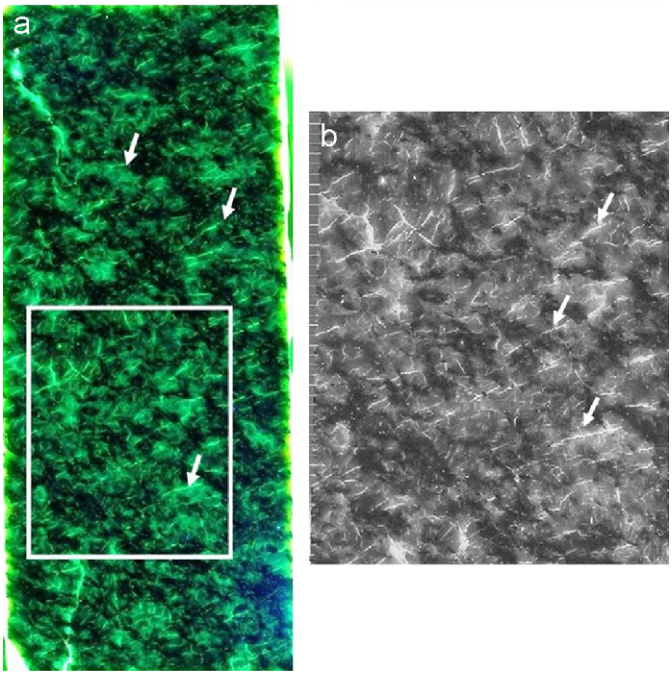

Fig. 3. (a) Sectioned specimen (126 × 51 mm) impregnated with fluorescent epoxy photographed before testing under UV lighting. (b) Enlarged portion of the specimen (size 44 × 33 mm), an mm scale can be seen to the left in the image. The fracture pattern is enhanced through image analysis. Arrows show location of pre-existing fractures.

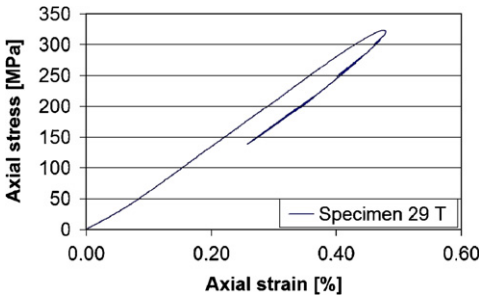

Fig. 4. Class II stress–strain curve for the specimen sections shown in Fig. 5. Note that the Ävrö granite is ultra-brittle, this being an extreme example of Class II behaviour.

As indicated by Fig. 6(a), the Ävrö granite was found to be extremely brittle, i.e. the descending portion of the complete stress–strain curve is close to the ascending portion, indicating that relatively little energy is required to continue the failure process. This is also reflected in the irregularity of the radial strain curves as the machine corrects for the individual rock failure events. On studying the individual curves, it was found that the post-peak behaviour, which follows Class II-type behaviour in all the specimens tested, was also affected by the fluid composition, as evidenced by the slopes of the post-failure loci. The general trend is that the slopes of the failure loci for several of the samples subjected to saline water have a higher

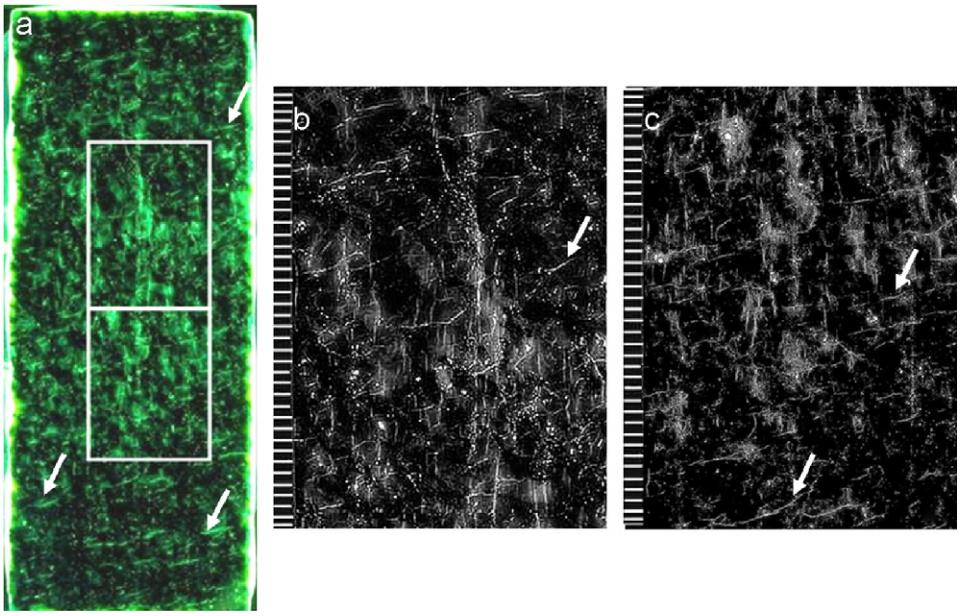

Fig. 5. (a) Sectioned specimen (126 × 51 mm) about halfway down the post-peak portion of the complete stress–strain curve (140 MPa) shown in Fig. 4. Specimen impregnated with fluorescent epoxy photographed after testing under UV lighting. (b) Enlarged portions of the upper white rectangles in (a). (c) Enlarged portions of the lower white rectangles in (a). Millimetre scales are shown to the left of each picture. The white cracks orientated across the page (indicated by arrows) are pre-existing cracks; the white cracks orientated down the page are those induced by the compressive loading in the laboratory.

positive slope than those for the specimens from the other groups (Table 1). The results indicate that a saline solution causes the rock specimens to be less brittle, i.e. tending towards Class I behaviour although is should be kept in mind that the number of samples are quite small and that there is a range for the results (Table 1).

The results from these tests, with the trends for unconfined compressive strength (UCS) and post-peak loci illustrated in Fig. 6(b) and the results presented in Table 1 show that the saturated specimens have a decrease in both elastic modulus and UCS compared to the dry specimens. A similar decrease of the UCS for these conditions has also been seen in many other studies [14–18]. Moreover, it can be seen that specimens saturated with saline solution exhibit a larger decrease in elastic properties than the specimens saturated with distilled water (Fig. 6(b)) when compared to the dry samples. The UCS of the specimens saturated with 0.68% or 10% saline solution are on average about 17% lower than the UCS of the dry samples. The salinity reduces the modulus and strength as to distilled water might be an indication of the effect of the salt at the crack tips affecting the crack tip surface energy and hence the stress required for crack propagation [11].

2.2. Strain-rate stepping test of Ävrö granite

Further physical testing in this campaign was related to time dependency of the mechanical behaviour of the specimens, bearing in mind the recommendations mainly from the ISRM suggested methods: ISRM SMs [12,19,20] which are related to the testing and saturation of the individual tests as presented here. Following the first set of results as just described, a second set of specimens was also subjected to uniaxial compression testing and the saturation recommendations of the standards were followed, but here the acoustic emission was also monitored during the structural breakdown of the samples. Some specimens were subjected to triaxial testing and indirect tensile tests (Brazilian tests) and some to study time dependency using 'strain-rate stepping' tests (controlled by constant axial displacement rate before the peak). These tests are described in [2].

During this second set of tests, a servo-controlled MTS 815 Rock Mechanics Testing System was used. As the results from the triaxial test are used to constrain the strain-rate stepping test the specimens for the triaxial and strain-rate stepping test were selected as close to each other as possible in order to minimize the heterogeneity between the specimens.

The strain-rate stepping tests were initiated at a confining stress of 7 MPa and 60% of the peak strength obtained from the triaxial testing. The peak differential stress value $\sigma_{\Delta po}$, inelastic strain rate $_{o}$ at peak stress and the critical inelastic strain (strain at fault nucleation or the non-linear component of total strain) ε_n are interpreted from the triaxial test results and utilized as reference values in the strain-rate stepping test. During the tests, the axial strain rates were varied from 10% to 0.1% of the strain rates from the triaxial tests, resulting in a stepwise stress increase. The apparent time-to-failure is estimated as the ratio between the critical inelastic strain from the triaxial tests, and the inelastic strain rate from the strain-rate stepping results at selected values of differential stress. As an example of results from these tests of the Ävrö granite,

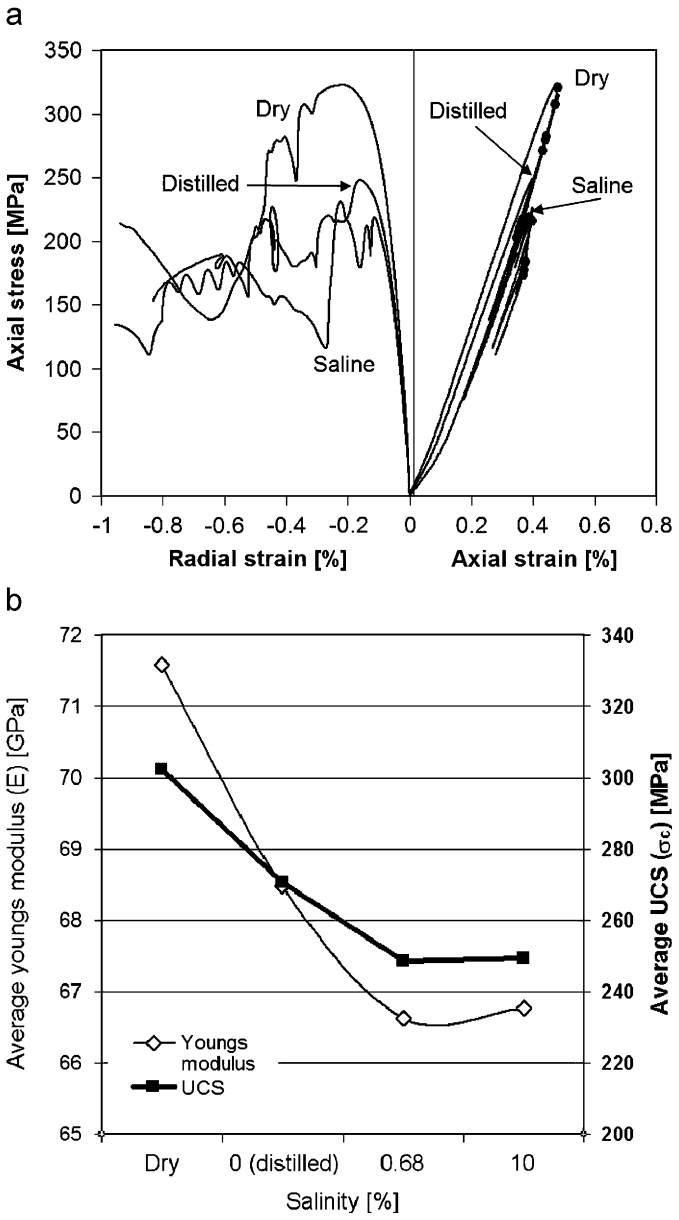

Fig. 6. (a) Class II stress–strain curves for three individual specimens subjected to the separate conditions of dry, distilled and saline water following 90 days immersion each. (b) Mean Young's modulus and UCS of the specimens for the same four saturation conditions. (The Young's moduli values are hollow diamonds with the axis shown on the left and the UCS values are the filled squares with the axis shown on the right).

one tested pair indicated that the time-to-failure increase from about 60 s at 265 MPa to about 20 days at 200 MPa and to 150 years at 150 MPa, these results are extrapolated from a 22 h test.

2.3. Fracture toughness tests on Ävrö granite

The third set of specimens was used to provide input information for one of the numerical modelling methods (FRACOD, described below). This involved the development of a new method to determine parameters describing

Table 1
Mechanical properties of the specimens as tested for different chemical conditions (after 90 days immersion)

Specimen group	Young's modulus (E) (GPa)	UCS (MPa)	+ve slope of the Class II post failure locus (GPa)
Dry			
Min	70.4	273.9	87
Mean	71.6	302.3	95
Max	72.7	335.8	111
Distilled			
Min	67.5	249.4	85
Mean	68.5	270.5	101
Max	69.4	287.4	111
Formation			
Min	66.1	232.8	84
Mean	66.6	248.5	97
Max	67.2	264.2	115
Saline			
Min	65.1	220.4	82
Mean	66.8	249.4	141
Max	67.8	277.0	209

sub-critical crack growth under tensile and shear stresses [2]. The parameters needed for the description of the sub-critical crack growth of intact rock are, *inter alia*, the constant (A) and the sub-critical crack growth index (n). These parameters are derived from the power law equation describing the velocity of the sub-critical crack growth by stress corrosion, described by [21]

$$v = AK^n, \tag{1}$$

where A is a constant, K is the stress intensity factor and n is the sub-critical crack growth index (or stress corrosion index). The stress corrosion index is a measure of the susceptibility of the material to stress corrosion cracking when subjected to a certain environment defined in the test (in this case distilled water during ambient temperature).

To obtain the sub-critical fracture parameters needed for the numerical modelling, both testing for Mode I (tensile) fracture toughness from the Chevron Bend test [22] and Mode II (shear) fracture toughness from the punch-through shear tests (PTS test) were performed [23,24]. The PTS test, together with the Weibull statistical method [25], was used to obtain the time-dependent behaviour from Mode II fractures and to calculate the Mode II fracture toughness.

To obtain all the parameters needed to assess the behaviour, two sets of tests on the same population are needed, similar to the strain-rate stepping tests in the second set of tests. In order to determine the Weibull distribution parameters, a series of rapid loading tests was performed, after which a series of constant loading tests on extra specimens of similar volume was made. All samples

Table 2
Results from the Modes I and II loading tests (notched three-point bending test and punch-through shear test), fracture toughnesses K_{IC} and K_{IIC} and stress corrosion index (n) for samples of Ävrö granite saturated with de-ionised water, from [2]

Parameters	
K_{IC} (MPa m$^{1/2}$)	2.7
K_{IIC} (MPa m$^{1/2}$)	4.5
$n_{(tensile)}$	48
$n_{(shear)}$	94

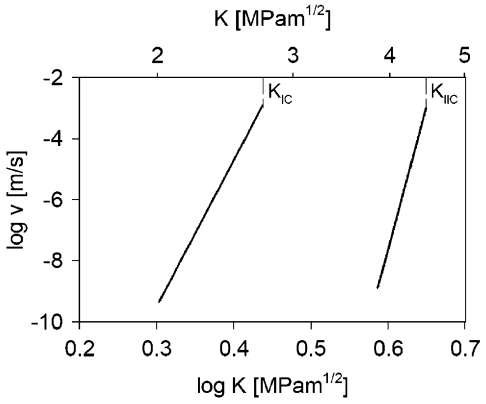

Fig. 7. Crack velocity (v) versus stress intensity factor (K) plot for Modes I and II sub-critical crack growth (data from [2]).

tested were saturated with de-ionized water at ambient temperature and pressure conditions; the experiments were carried out in a stiff servo-controlled MTS loading machine with a force capacity of 4600 kN, with high accuracy load cells in the ranges 0–25 and 0–1000 kN being used.

The parameters reported from these tests are: the Mode I and Mode II fracture toughness (K_{IC} and K_{IIC}) and the stress corrosion index for both tensile and shear fractures (Table 2). From the resulting plot of crack velocity and stress intensity factor data for Mode I and Mode II loading conditions, shown in Fig. 7, it can be seen that a lower stress intensity is needed for Mode I compared to Mode II loading to achieve the same fracture propagation.

The fracture toughness for specimens saturated with de-ionized water is 12% lower than the fracture toughness for dry samples of the same rock type from an earlier testing campaign [23]. This shows similarity to the results found in the uniaxial compression tests for dry conditions and saturated conditions as reported earlier in this paper as well as the results from [26].

3. The four numerical methods used to simulate rock failure in uniaxial compression

Several numerical approaches have been developed to simulate the degradation and failure of intact rock. In this study, representatives of both continuum- and discontinuum-based modelling tools are presented. The continuum approach is based on the application of fundamental models such as the elasto-plastic/elasto-viscoplastic models (e.g. [27]) and damage mechanics models (e.g. [28]). When these models are applied to large deformations and failure, a number of parameters are required that are difficult to measure directly through physical testing. This causes a special approach when simulating discontinuities with a continuum-based model [29]. The discontinuum-based models usually incorporate more direct and hence simplified assumptions based on the constitutive behaviour of the rock matrix and fractures. They can be developed from empirical observations of the behaviour of rocks (like FRACOD with pre-existing cracks) or via particle mechanics (such as the Particle Flow Code (PFC) involving a series of discrete elements).

In both approaches, several parameters relating to the microscopic mechanical behaviour of the rock are needed and it is impossible to measure these today with physical test methods. For example, it is not practically possible to determine the crack length and orientation of the most critical crack from a rock specimen (used as input into FRACOD). The smaller the crack, the higher is the stress needed to trigger fracture propagation. In FRACOD, the assumption of the size of an initiated crack is equivalent to that of the largest flaw expected in the material, whereas, in the PFC a representation of the rock at grain scale can be produced and the central finite difference method, as applied in the distinct element method (DEM), is used to calculate the movement and interaction of each particle. This method can mimic a cemented granular material from which the damage process can be observed.

The four numerical modelling techniques used for the simulations were (a) the elasto-plastic cellular automaton (EPCA); (b) the particle mechanics approach—the PFC; (c) the displacement discontinuity method (DDM)—the FRACOD code; and (d) the finite element method (FEM)—the damage expansion model. In the following sections, we describe each of these in turn and we highlight the associated simulation results.

3.1. The elasto-plastic cellular automaton (EPCA) simulation

This model simulates the rock behaviour in 2-D. The rock specimen is divided into a system of cell elements and, to describe the heterogeneity of the rock matrix, the mechanical properties for each element, such as Poisson's ratio, Young's modulus cohesive strength, etc., are distributed by characterising them with the Weibull probability density function [25]. To describe the heterogeneity of the material, a homogeneity index (m) is used.

In the EPCA method, three control methods can be considered, i.e. stress loading, constant strain rate and the linear combination of stress and strain. To control the loading process for Class II behaviour during uniaxial

Table 3
Mechanical and loading parameters for the EPCA simulation of the physical tests

Parameters	Value and unit	Parameters	Value and unit
Young's modulus	68 GPa	Residual coefficient	0.1
Poisson's ratio	0.3	CA iterative precision	$1e^{-7}$
Compressive strength	234 MPa	Softening coefficient	0.05
Tolerance	1%	Random seed	10 and 15
Homogeneity index	6.0	C	$3.9e^{-5}$
E/E'	0.5		

compression, a linear combination of stress and strain was used for the control programme as developed by Okubo and Nishimatsu [30] and further described in [31].

This linear combination of stress and strain can be expressed as

$$\varepsilon - \frac{\sigma}{E'} = Ct, \tag{2}$$

where σ is the stress, ε is the strain, and the E' and C are a fixed chosen modulus value and the loading rate, respectively, t being time.

In each loading step, the cell state is updated according to the cellular automaton updating rule [32]. The cell elements follow the elasto-plastic loading and unloading rule [32,33]. This is a function of the softening coefficient (α), which determines whether the stress–strain curve will follow the monotonic strain case (Class I behaviour) or the non-monotonic strain case (Class II behaviour), following the equation

$$0 < \alpha \leqslant 1 - \beta, \tag{3}$$

where β is the residual strength coefficient of the yield surface at each step. For the non-monotonic strain case, $\alpha = 1-\beta$; whereas $0 < \alpha < 1-\beta$ for the monotonic strain case.

At each step, the updated stresses are substituted into the failure criterion, such as the Mohr–Coulomb or Drucker–Prager criteria, to verify whether the strength criterion is met or not and hence if yielding of the cell element will occur. If the cell element yields, it follows a corresponding plastic strain according to the elasto-brittle-plastic constitutive theory [34–36]; otherwise, the external force is increased further. The stress and deformation distribution throughout the specimen model are then adjusted after each rupture to reach the equilibrium stage.

To simulate the behaviour of the Ävrö granite, specimens subjected to a saline solution during a uniaxial compression test, the test was simplified as a plane stress model and a vertical section was considered. Due to the Class II behaviour of Ävrö granite under uniaxial compression, the linear combination of stress and strain was used as the loading control method in the model. The

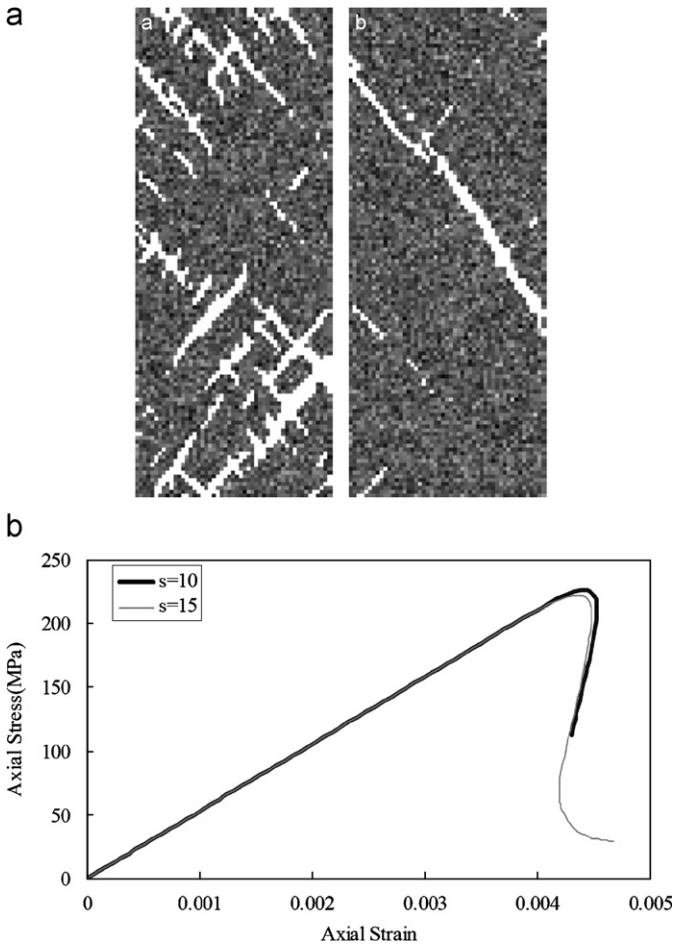

Fig. 8. (a) Illustration of the fracture development from the EPCA simulation of the saline experiment with two different elemental seeds: (i) seed = 10 and (ii) seed = 15. (b) The resulting complete stress–strain curves for the simulation with different seeds of the uniaxial compression of samples subjected to a saline fluid.

mechanical parameters considered as identified from the laboratory test, are presented in Table 3. The model-specific parameters are: homogeneity index $m = 6$; the E/E' as 0.5 (where E is the modulus and E' is a fixed modulus derived from the linear combination of stress and strain), and the random elemental seeds of 10 and 15 were used. The Drucker–Prager criterion was used as the yield criterion and the test was simulated with a fixed lower sample end and the upper end was loaded according to the linear combination of stress and strain control.

From the results (Fig. 8(a)), it can be seen that the failure pattern is different in the two simulations with different seed parameters but, when considering the stress–strain response from the simulations in Fig. 8(b), then it can be seen that the two simulations do successfully reproduce a similar Class II behaviour. In this study, it was found that the resulting compressive strength is more influenced by the homogeneity index than the seed number; whereas, the opposite applies for the failure mode of the rock.

3.2. The Particle Flow Code (PFC)

The particle mechanics code applied is the Particle Flow Code (PFC^{2D}) [37–40], which simulates the mechanical behaviour of a rock material represented as an assemblage of many small rigid circular particles bonded together. The movement and interaction of each particle is calculated using the central finite difference methods as applied in the DEM. For the models of contacts, both linear and non-linear (Hertz) contact models with frictional sliding can be used. The linear contact model, which was used in this study, provides an elastic relation between the relative displacement and contact force of particles.

In this method, the stage of back-calculation of micromechanical parameters (such as contact stiffness and strength at the grain boundaries) from the macro-parameters obtained from physical laboratory measurements is needed. The microparameters required are: particle radius, stiffness of particle contacts, friction coefficient between particles, and normal and shear strength of bonds. These microscopic parameters are unique for every approach as they have to be obtained from the macroscopic mechanical parameters by a calibration of the particle model with identical boundary conditions. This approach demands assumptions of particle size, contact model and initial particle packing configuration. The question of particle size depends on the scale dependency of the mechanical parameters of rock, such as the deformability and strength. Therefore, an investigation of the representative elementary volume (REV) for the Ävrö granite has been made to identify the proper particle size to use in this simulation. From this investigation, it was found that the coefficient of variation of mechanical properties decreases with an increase of the model size, but increases with particle size [41]. In the PFC code, cemented contacts are called parallel bonds. A parallel bond uses a set of elastic springs uniformly distributed over a rectangular cross-section lying on the contact plane and centred at the contact point. These springs act in parallel with the linear point-contact springs. Relative motion at the contact causes an incremental force and moment to develop due to the parallel bond stiffness.

A microcrack can thus be initiated by overcoming the stiffness of the bonds and hence causing breakage of the bond. Propagation is the progressive breakage of juxtaposed bonds.

When simulating the chemical degradation of the physical tests, all physical UCS tests were simulated individually. The microscopic parameters were calibrated for each group of specimens, subject to conditions of: dry, distilled, formation and saline hydro-chemical environment; Table 4. In this study, the uniaxial compression was simulated as the horizontal boundaries (upper and lower walls) moving slowly. The resulting axial stress and strain are derived from calculated contact forces and particle displacement. The UCS is the maximum value of axial compressive stress at peak compression load during simulation, which was calculated from the contact forces between the particles in the PFC models. The PFC approach does not use stress and strain as basic variables as in FEM. Instead, it uses contact forces and displacements/velocities of particles as basic variables, which can be used to derive equivalent stresses, strains and their rates as induced variables through averaging. The simulated specimen undergoes monotonic compression with controlled monotonic increase of axial strain without unloading or addition of lateral strain constrains; this means that Class II behaviour cannot be modelled by PFC in this control mode.

When comparing the microscopic parameters calculated from the physical testing, the variation between the Young's modulus for bond-to-bond strength can be a result of the chemical effect noticed in the physical tests. The decrease in uniaxial compressive strength observed in the laboratory tests can be interpreted as the chemical weakening of the contact bonds' normal and/or shear strengths, although, no clear trend can be discerned [42].

In the results from the simulations, Class I behaviour is obtained because of the monotonic axial strain increase used to control the mechanical evolution for all specimens

Table 4
Microscopic parameters of PFC^{2D} model for selected samples

Parameters	Dry_18	Saline_13	Distilled 40_24	Distilled 90_07	Formation 40_30	Formation 90_20
Ball density (kg/m^3)	2670	2670	2670	2660	2680	2660
Minimum ball radius (mm)	0.35	0.35	0.35	0.35	0.35	0.35
Ball size ratio	1.5	1.5	1.5	1.5	1.5	1.5
Number of balls	8898	9055	8905	8891	9501	9090
Ball–ball contact Young's modulus (GPa)	70	74	85	73	76	79
Ball stiffness ratio	4	5	6	5	4.5	6
Young's modulus of parallel bond (GPa)	70	74	85	73	76	79
Parallel bond stiffness ratio	4	5	6	5	4.5	6
Particle friction coefficient	0.5	0.5	0.5	0.5	0.5	0.5
Parallel bond normal strength, mean (MPa)	502	485	630	550	567	628.5
Parallel bond normal strength, std. dev. (MPa)	0	0	0	0	0	0
Parallel bond shear strength, mean (MPa)	125.5	97	105	110	126	104.5
Parallel bond shear strength, std. dev. (MPa)	0	0	0	0	0	0

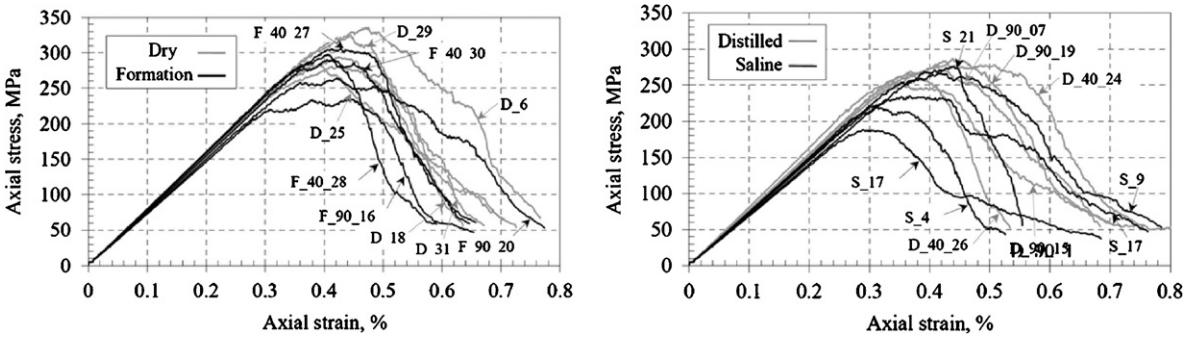

Fig. 9. Complete stress–strain curves for the simulation of the physical tests of Ävrö granite subject to different chemical porewater conditions where (left) the letter D is for specimens under dry conditions, and F is for specimens saturated with formation water and (right) the letter D is for the specimens saturated with distilled water and *S* for the specimens saturated with saline water. In the specimen coding, e.g. F 40 30, the letter refers to the water condition, the first number refers to the number of days of saturation, and the second number refers to the specimen number [2].

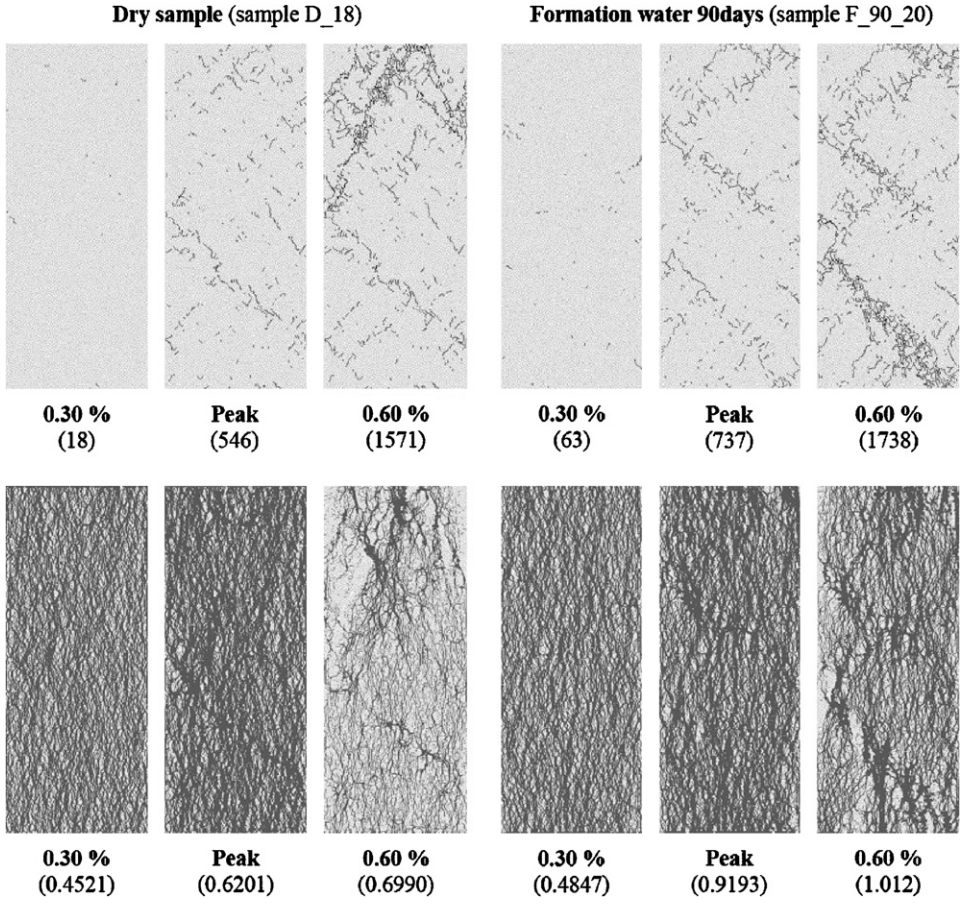

Fig. 10. Fracture evolution (top) and contact force distribution (below) at: before peak (0.3% strain), at peak, and after peak (0.6% strain). The values in parentheses are the number of the microcracks (top) and maximum contact force, MN (below) [2].

(Fig. 9). In these simulations of the physical testing, no clear effect on the micromechanical parameters from the chemical damage could be discerned.

The complex degradation process in the pre- and post-peak stress behaviour of intact rock can be simulated with the PFC approach (seen in Fig. 10) including crack initiation, growth, coalescence, localization and complete breakdown without requiring continuous system re-configuration. When looking at the predicted progressive development of microcracks and contact force distributions for a simulation of a specimen under dry conditions as well as a simulation of a specimen saturated with formation water (Fig. 10), the formation of multiple shear-band-like localized zones appear to be the main cause of damage and failure.

3.3. The displacement discontinuity method (DDM)

In the FRACOD code, based on the DDM [43], discontinuities in the rock are simulated using DDM elements for opposite surfaces of the discontinuity. This 2-D model can predict the fracturing processes including fracture initiation, fracture sliding/opening and fracture propagation. Both tensile (Mode I) and shear (Mode II) failure are considered [44]. FRACOD considers the intact rock as a homogenous and flawless elastic body. New cracks are implemented in the model indicating micro-structural processes in critical stress locations leading to macrocrack formation.

Fractures are initiated as potential failure surfaces in the direction perpendicular to the tensile stress where the tensile stress reaches a pre-defined portion of the tensile strength for the intact rock. To describe shear failure, the cohesion and friction angle from the Mohr–Columb criterion are used to define the potential failure plane. When such a plane is initiated, it can either slip or open, and its cohesion will drop to zero. FRACOD uses a probabilistic approach to simulate fracture initiation depending on the stress/strength ratio [2]. To describe fracture propagation, the Griffith G-criterion is used with the extensions suggested by Shen and Stephansson [45], termed the F-criterion. The direction of the fracture propagation will correspond to the direction where the F-value is at its maximum according to

$$F(\theta) = \frac{G_{\mathrm{I}}(\theta)}{G_{\mathrm{IC}}} + \frac{G_{\mathrm{II}}(\theta)}{G_{\mathrm{IIC}}}, \tag{4}$$

where G_{IC} and G_{IIC} are the critical strain energy release rates for Mode I and Mode II fracture propagation, $G_{I}(\theta)$ and $G_{II}(\theta)$ are strain energy release rates due to the potential Mode I and Mode II fracture growth of a unit length. The F-criterion can be determined from the strain energy release rate of Mode I and Mode II at a given fracture tip [2].

A uniaxial compression test was simulated with the mechanical parameters from several physical tests where the specimens have been saturated with distilled water [11,23,46] (Table 5). The two main parameters used in the FRACOD model are the fracture toughness and the crack length. They define the level of stress at which the crack starts to propagate. The initial crack length is determined from a numerical sensitivity analysis under these conditions with varying crack lengths. The initial crack length was set to 3.125 mm in this simulation.

In FRACOD, the stress and strain change can be monitored at any point within the numerical model during the loading–unloading process. In this simulation, the stress was monitored at the top of the specimen. The radial response was monitored at four locations on the vertical boundary.

At the start of the simulation, the axial strain was applied in each small step (0.0016%), equivalent to about a 1 MPa increase in the elastic region. After the peak strength, a reversal of the axial strain was applied to be able to simulate the Class II behaviour when unstable fracture propagation started. The fracture initiation level was set to start at a stress level of 121 MPa, which is the crack initiation strength from physical tests. As seen from the results of the simulation, the stable fracture propagation starts at a stress level of 225 MPa and, at peak strength for the rock (232 MPa), unstable fracturing ensued (Figs. 11 and 12). To simulate Class II behaviour, the unloading was started after passing the peak strength. The progressing failure is detected as increasing radial strain, even if the axial strain is kept constant or even reduced (see Fig. 12).

Table 5
Input data for numerical simulation of uniaxial compression tests using FRACOD

Parameters	Values and units
Intact rock	
Young's modulus	68.0 GPa
Poisson's ratio	0.24
Cohesion	31 MPa
Friction angle	49°
Tensile strength	14.8 MPa
Crack initiation strength (for UCS)	121 MPa (from AE measurements)
Fractures	
Size of newly initiated crack	3.125 mm
Fracture toughness Mode I	3.21 MPa $m^{1/2}$
Fracture toughness Mode II. No confinement	4.6 MPa $m^{1/2}$
New crack stiffness: K_n and K_s	26,976 GPa/m
Friction angle	49°
Cohesion, before and after sliding	31 MPa, 0 MPa
Dilation angle	5°
Initial fracture aperture	10 μm
Residual fracture aperture	1 μm

The reproduction of the behaviour of Ävrö granite indicate that even at a relatively small confinement, the tensile fracture propagation is restrained which benefits the shear fractures for Ävrö granite, although shear failure seems to be the dominating failure mode even under simulated uniaxial loading.

A sensitivity analysis conducted in connection with this study indicated that the post-peak behaviour of the rock is strongly affected by the loading configuration, material properties, etc. The unstable fracturing process of Class II behaviour may also cease when a propagating fracture reaches another.

3.4. The finite element method (FEM)—damage expansion model

The essence of the damage model is that during microstructural failure, the local elastic modulus is given by the proportion of surviving elements multiplied

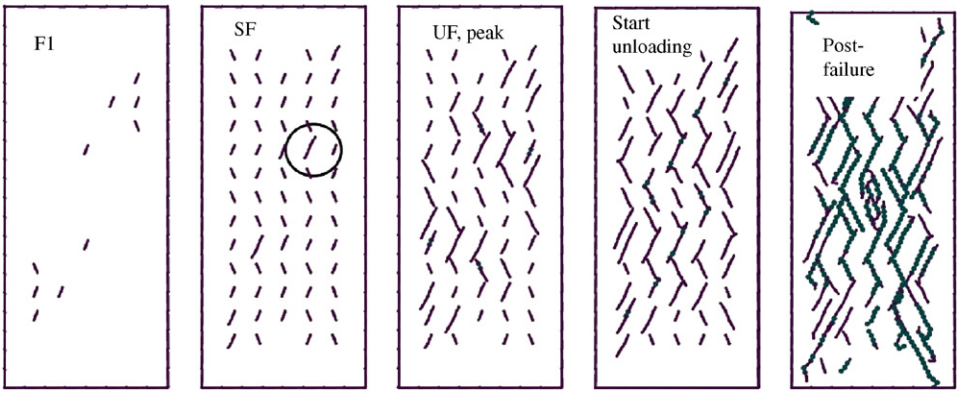

Fig. 11. The simulated fracture pattern at; fracture initiation (FI), stable fracture propagation (SF), unstable fracture propagation (UF), unloading at the peak stress, and the continuation of cracking.

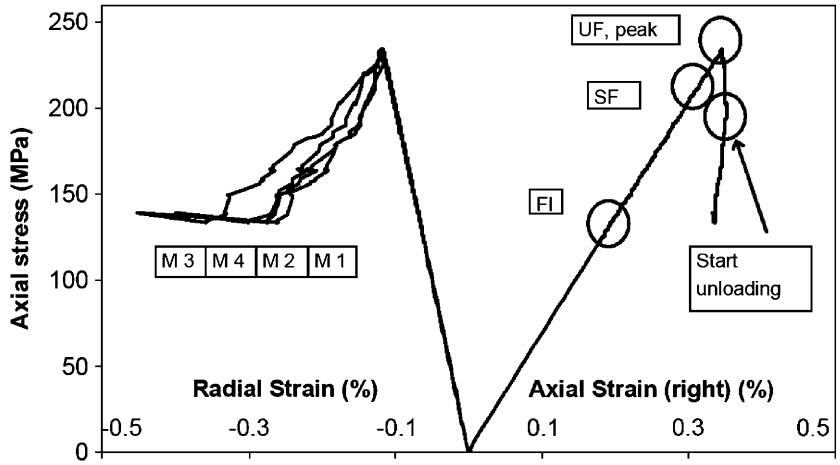

Fig. 12. Simulated stress–strain curve illustrating the failure behaviour via both radial and axial strains. The situation represented by FI, SF, UF and start unload can be seen in Fig. 11.

by the original modulus value—a concept developed from the earlier work of Hudson and Fairhurst [47]. This is the only 3-D simulation method in the study and, in this continuum simulation technique, not only is conventional damage mechanics used but, in addition, the volume change due to damage development is calculated.

In this method, termed the damage expansion model, the damage is increased by the additional strain energy, but is not changed during the unloading process. To be able to simulate fracture growth, the damage variable D is used (i.e. the proportion of damaged elements), which in turn is comprised of several damage parameters [47], these parameters describing the initial and progressive condition of the damage are derived from test results such as axial stress and strain, tangential strain, Young's modulus (E_0) and Poisson's ratio at initial loading (v_0) [2]. The damage parameters are: B_0, the initial damage potential; K_v and K_d, the proportional constant of damage potential to volumetric strain and damage variable; n_v and n_d are scaling factors of the volumetric strain and damage variable, respectively, and D is the damage variable; more information of their interrelation can be found in [2,48]. Whereas K_d and n_d are related to the strength, both parameters do not have any effect on the behaviour of volumetric strain. When K_d is small or n_d is high, the strength becomes high. On the other hand, K_v and n_v are not related to the strength. When K_v is small or n_v is large, the behaviour becomes brittle, which induce a drastic softening and increase of volumetric strain. By combining the four parameters, any typical behaviour can be represented.

During simulation using this method, the Class II behaviour described by Wawersik cannot be discerned directly, but the behaviour can be mimicked based on the assumption that Class II behaviour can be described via the excess energy being used only for fracture propagation, which makes the energy consumption a phenomenon localized to the fracture; however this is not exactly the same as the Class II behaviour described by Wawersik [4], although the observed behaviour is similar.

The chemical effect is implemented as changes in the damage parameters derived from the results of the laboratory tests.

Table 6
Damage parameters derived form the laboratory tests for the three simulated cases [2]

	K_d (MPa)	n_d	K_v (MPa)	n_v	B_0 (kPa)	E_0 (GPa)	v_0
Distilled	1.2	0.5	141	0.8	225	57	0.2
Saline	1.7	0.8	106	0.95	180	60	0.23
Longer time for saturation	2.0	1.0	70	1.1	135		

The geometry of the laboratory samples was followed in the simulation. The lower end of the specimen has roller conditions and it is at the upper end where displacement is initiated. The stress is obtained as the mean equivalent nodal stress at the top boundary. The strain is calculated symmetrically around the central lateral axis with a distance of 50 mm.

For the simulation of the chemically degraded specimens, three cases were tested: the specimens subjected to distilled water; the specimens subjected to saline water; and a case with intensified damage. To introduce heterogeneous energy consumption, an initial defect is pre-defined at the top of the specimen. This is a representation of the edge disturbance from cutting the specimen. The region is a 1 mm thick part of the cylinder representing the specimen where the initial damage parameter (D_0) is set to 0.01. The other parts of the model have no initial damage.

The damage parameters used for the case of specimens subjected to distilled and saline water are derived from the laboratory tests presented earlier (Table 6). The intensified damage parameters were used in the last case to simulate a longer time of sample immersion in saline water (Table 6).

As seen in Fig. 13, the different damage parameters calculated from the physical tests vary. The increase in K_d and n_d did not induce a large change in peak strength, whereas the decrease in K_v and the small increase in n_v would indicate a more brittle behaviour, sharp peak and abrupt increase of volumetric strain. However, the strain at the peak stress may not be changed much due to the decrease in K_v being counteracted by the increase in K_d. Besides, when the initial damage potential (B_0) decreases, the development of damage will occur at an early stage; this may introduce early failure leading to lower strength [2].

The results for the three cases are shown in Fig. 13. The decrease of the peak strength of the specimens subject to chemical degradation (seen in the right part of Fig. 13) is likely a result of the decrease of the initial damage potential (B_0). When comparing the post-peak behaviour of the cases, development of damage can be seen in the inner part of the specimen in the case of the distilled water; whereas, the damaged area developed in the outer part of the specimen resulting in intensified damage.

In these simulations, it can be seen that the modelling of the specimen containing distilled water displays damage development at the centre of the specimen; whereas, in the simulated specimen with intensified damage parameters, the damage is enhanced close to the edges of the specimen. To simulate Class II behaviour, a new constitutive law characterising unstable damage development in the post-peak region must be established.

One of the items relating to the complete stress–strain curve is that it was clear from these simulations that the local stress–strain considered at different locations on the specimen are different. However, it is the overall engineering stress–strain curve for the complete rock element that is being considered here.

4. Realism of the model simulations and discussion

We began this paper by explaining that the overall motivation and the specific context of the modelling and testing programme was to evaluate the consistency and validity of four numerical models as applied to the simulation of the complete stress–strain curve for Ävrö granite tested in uniaxial compression. The first approach to the results was to summarize the capabilities of the model and to consider their consistency. The models' capabilities are listed in Table 7.

We have presented the experimental results and the numerical modelling results, plus a listing of the different models' capabilities, and we can now address the objective of the paper: to what extent are the numerical models consistent and valid?

All the four modelling methods are able to reproduce Class I behaviour where the strain monotonically increases but it is harder to model the 'snap-back' Class II behaviour where the strain does not monotonically increase. The Ävrö granite is ultra-brittle and its behaviour in uniaxial compression is strongly Class II. In this exercise, and for the laboratory test conditions, the EPCA model, and the DDM technique represented by the FRACOD model managed to reproduce Class II behaviour. Although the exact test conditions and results could not be faithfully simulated, the general trends in mechanical behaviour were apparent from the models. The Class II behaviour was not simulated by the PFC model at this stage in its current form, but such behaviour can be simulated by using appropriate numerical control techniques. The damage expansion model was able to be adapted through the extraction of strain energy to approximate the Class II behaviour in the uniaxial compressive test.

The discontinuous, inhomogeneous and inelastic nature of rock material can be simulated using the EPCA model, through the ability to incorporate initial failed elements, the use of the homogeneity index, the random seed of the mechanical parameters for cells and the possibility to

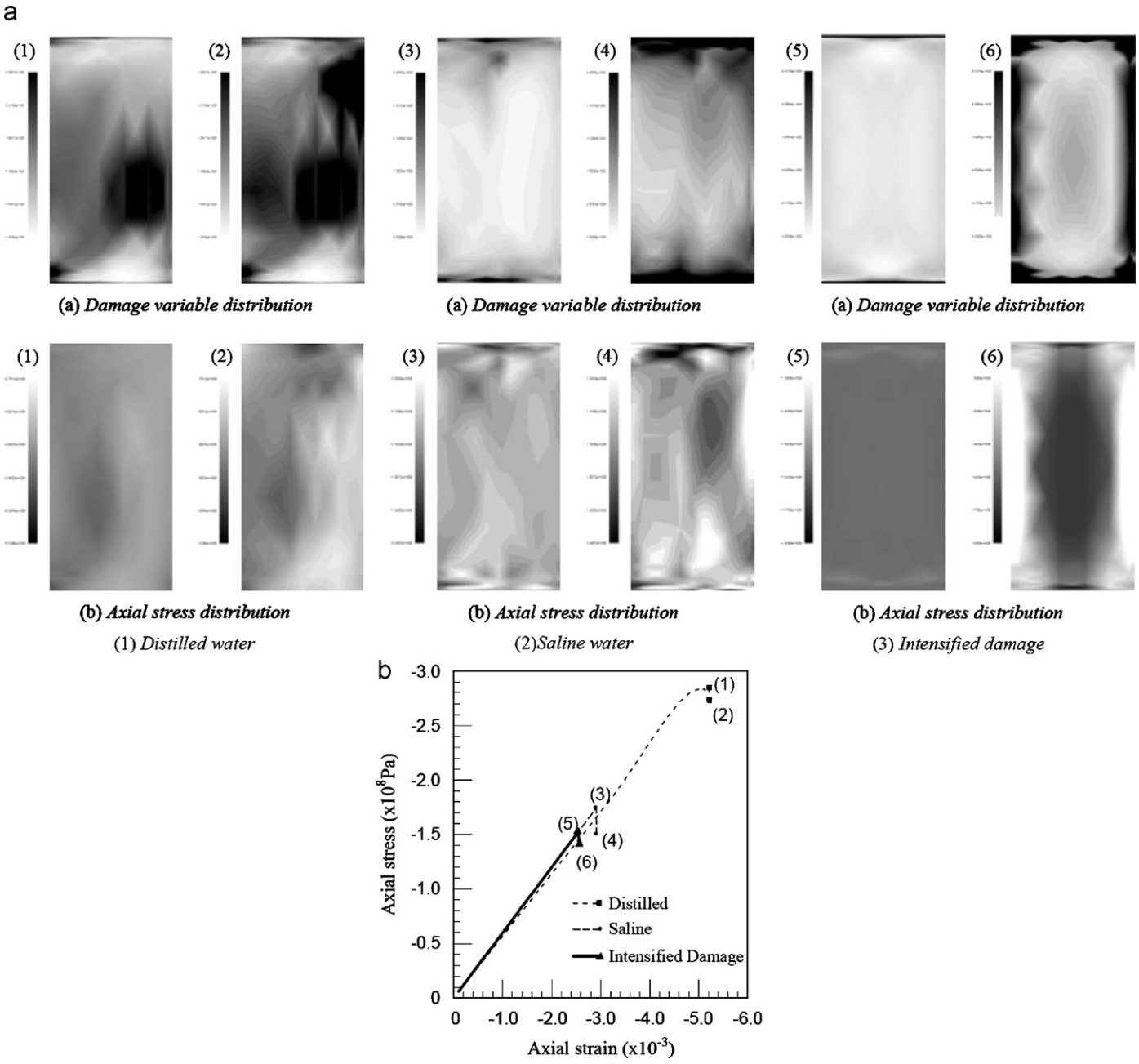

Fig. 13. The results of the three FEM cases simulated, where the distribution of the damage and the axial stress are seen in (a) (with large damage and high axial stress represented by increased grayscale) and the calculated stress–strain relations are shown to the right (b). The numbers in the two parts refer to the situation just before the peak and just after the peak for the different cases.

implement several different control methods. It is crucial to identify the correct elemental yielding criterion in this method to be able to reproduce the behaviour of rock failure. The post-peak behaviour is controlled using the softening coefficient.

The PFC model, based on elemental discs or spheres, is also able to model the discontinuous, inhomogeneous and inelastic nature of the rock through the geometrical set-up and the interactions between the elemental particles. It shares the disadvantage common with the EPCA and damage models that the parameters of the numerical model are not directly measurable by laboratory tests. However, this modelling technique is particularly instructive in terms of the mechanisms that it demonstrates.

The same comments apply to the damage model approach which can be modified to incorporate a variety of features, but the 'sub-parameters' used to express the damage proportion for various conditions cannot be measured directly via laboratory tests.

The advantage of FRACOD is that many of the parameters can be directly measured by physical tests and they all have physical meanings, derived directly from linear elastic fracture mechanics (LEFM) together with sub-critical crack growth theory. Fracture initiation, stable

Table 7
Summary of the capabilities of the four numerical models used in this study

Parameter	Models			
	Elasto-plastic cellular automaton model	PFC model	Finite element damage expansion model	FRACOD—DDM model
Inhomogeneity, rock material and cracks	Yes, using Weibull distribution of properties	Yes different particle sizes, different contact bond strengths and stiffnesses	Yes, different damage for D, but intact part is homogeneous	Yes, multiple intact rock domains/presence of cracks
Type of failure (Class I)	Yes	Yes	Yes	Yes
Type of failure (Class II)	Yes	Not implemented, but possible	Yes, but indirectly	Yes
Chemistry	Yes, via element changes	Yes, via changing the particle bonds	Yes, via intensified damage	Yes, via changing crack propagation velocity (Charles' law)
Anisotropy	*Yes, via cell property specification*	*Yes, via the particle specification*	*Yes, via specification of the elements*	*Yes, via crack orientations or via directional material properties e.g (not implemented)*
Pore pressure	*Yes, via effective stress*	*Yes*	*No, but could be implemented in the future*	*Yes, via application of static pressure in the fracture, but uncoupled*
Time dependency	*Yes, via changing the properties with model steps, also can use viscous elements*	*Yes*	*Yes, but has not yet been done*	*Yes, via crack propagation velocity (Charles' law)*
Fractures	*Yes*	*Yes*	*Yes, but have to be considered separately*	*Yes, several fracture properties can be incorporated*
Temperature	*Yes*	*Yes*	*Yes, but not yet*	*Not directly*

The first four completed rows represent capabilities that were used in the current modelling; the last six italicised rows represent further model capabilities.

and unstable states of fracture, peak strength and post-peak behaviour, including Class II behaviour, have been successfully modelled. An important advantage of this code is its capability to realistically model the brittle axial and lateral strain responses during the failure process.

A change in the macroscopic mechanical properties could be seen in the physical testing performed with different hydro-chemical conditions for the specimens of the crystalline rock type: Ävrö granite. The data are unfortunately rather limited and no definite conclusions on the distinction between chemical effects and heterogeneity in the rock material could be made. Nevertheless, all four research groups used their models in different ways in their attempts to simulate the effects of the different porewaters. It is clear that the potential is there for simulation and associated sensitivity studies of the chemical effects: the problem is to obtain appropriate parameters characterising the chemical effects at the microscale for input to the numerical models.

5. Conclusions

Testing of the Ävrö granite under servo-controlled conditions in uniaxial compression indicated an ultra-brittle rock type with a strong Class II behaviour in which the strain does not monotonically increase.

Limited testing of specimens under dry conditions, saturated with formation and saline waters, showed that the presence of porewater affected the elastic modulus, compressive strength, and geometry of the complete stress–strain curve.

Four numerical models were used to simulate the progressive structural collapse of the rock microstructure in uniaxial compression: an EPCA code, the 2-D PFC, FRACOD based on the DDM, and a damage expansion model based on the FEM. All these models were useful in characterising and illustrating the trends in mechanical behaviour during the rock's microstructural breakdown. Moreover, all the models were suitable for sensitivity studies to evaluate the influence of their respective supporting parameters. In this context, the work has further demonstrated the value of numerical models as a research tool.

However, this work has also shown that there are still large issues in failure of rock displaying Class II behaviour under uniaxial compression tests that need to be addressed. The different models operate on different constitutive bases and the laboratory testing still needs to be developed to identify the damage and failure mechanisms of the intact Ävrö granite. The reproduction of the Class II behaviour that was achieved by some of the models must be regarded as a starting point for further development of the understanding of this phenomenon.

The modelling of rock deformation is a difficult subject and one in which the different numerical models describing the behaviour of the complex deformation and failure

process on the laboratory scale have displayed different advantages and disadvantages. These differences indicate that this subject is not fully understood and thus the simulation of *in situ* rock mass behaviour, where a plethora of further complications is added to the geometrical and mechanical aspects of the problem, needs to be approached with care.

Further work is required to consider the ways ahead in ensuring that numerical modelling studies have the best chance of adequately supporting engineering design. It is currently by no means apparent that such modelling is sufficiently realistic for all the problems they are applied to. In particular, an auditing approach is required which should be conducted concurrently with the modelling.

Acknowledgements

The authors are grateful to the Japanese Atomic Energy Agency (JAEA), the Radiation and Nuclear Safety Authority in Finland (STUK), Swedish Nuclear Fuel and Waste Management Co (SKB), and the Swedish Nuclear Power Inspectorate (SKI) for funding this research. The authors are also grateful to the support from the National Nature Science Foundation of China under Grant nos. 50709036, 40520130315. Rolf Christiansson of SKB is especially thanked for his most helpful support and facilitation of the experimental work. The advice of Ivars Neretnieks of KTH in Stockholm on chemical matters was invaluable. Additionally, Flavio Lanaro is gratefully acknowledged for his suggestions for improvement, and Lars Jacobsson of the SP Laboratory in Borås, Sweden, is thanked for his guidance and assistance with the laboratory test programme. Finally, the authors would like to thank Mariusz Kalinowski, Lars Mellin and Göran Olsson at Cement och Betong Institutet (CBI) for their preparation for the fracture analysis of some of the specimens.

It is emphasized that the views expressed in this paper are solely those of the authors and cannot necessarily be taken to represent the views of any of the organizations or individuals listed above.

References

[1] Hudson JA, Harrison JP. Engineering rock mechanics: an introduction to the principles. Oxford: Elsevier; 1997. 444pp.

[2] Hudson JA, Jing L. DECOVALEX-THMC-Task B. Understanding and characterizing the Excavation Disturbed Zone (EDZ)-Phase 2 report. Swedish Nuclear Power Inspectorate report (SKI) 2007; p. 104. (Available from 〈www.ski.se〉 and 〈www.decovalex.com〉).

[3] Wawersik WR. The value of laboratory experiments for code validations. Int. J Rock Mech Min Sci 2000;37:307–16.

[4] Wawersik WR. Detailed analysis of rock failure in laboratory compression tests. PhD thesis, University of Minnesota, 1968, 165pp.

[5] Wawersik WR, Fairhurst CA. Study of brittle rock fracture in laboratory compression experiments. Int J Rock Mech Min Sci 1970;7(5):561–75.

[6] Emsley S, Olsson O, Stenberg L, Alheid H-J, Falls S. ZEDEX—a study of damage and disturbance from tunnel excavation by blasting and tunnel boring. Swedish Nuclear Fuel and Waste Management Co (SKB). Technical report 97-30, 1997, 198pp.

[7] Martino JB, Chandler NA. Excavation-induced damage studies at the Underground Research Laboratory. Int J Rock Mech Min Sci 2004; 41(8):1413–26.

[8] Autio J, Malmlund H, Kemppainen M, Oila E, Siitari-Kauppi M. Study of rock damage caused by drill and blast excavation at Äspö hard rock laboratory. Posiva working report 2004a;2004–33.

[9] Autio J, Malmlund H, Siitari-Kauppi M. Study of rock damage caused by tunnel boring at Äspö hard rock laboratory. Posiva working report 2004b;2004–32.

[10] Janson T, Ljunggren B, Bergman T. Modal analyses on rock mechanical specimens, specimens from borehole KLX03, KLX04, KQ0064G, KQ0065G, KF0066A and KF0069A. Swedish Nuclear Fuel and Waste Management Co (SKB). Progress report 07-03, 2007.

[11] Bäckström A, Lanaro F, Christiansson R. Coupled chemical-mechanical behaviour: the influence of salinity on the uniaxial compressive strength of the Småland granite, Sweden. In: Proceedings of the second international conference on coupled-thermo-hydro-mechanical-chemical processes in geosystems and engineering (GeoProc 2006) 2006, p. 437–43.

[12] Fairhurst CE, Hudson JA. Draft ISRM suggested method for the complete stress–strain curve for intact rock in uniaxial compression. Int J Rock Mech Min Sci 1999;36:279–89.

[14] Price NJ. The compressive strength of coal measure rocks. Coll Eng 1960;37:283–92.

[15] Feucht LJ, Logan J. Effects of chemically active solutions on shearing behavior of a sandstone. Tectonophysics 1990;175:159–76.

[16] Karafakis MG, Akram M. Effects of chemical solutions on rock fracturing. Int J Rock Mech Min Sci 1993;30(7):1253–9.

[17] Feng X-T, Chen S, Li S. Effects of water chemistry on microcracking and compressive strength of granite. Int J Rock Mech Min Sci 2001;38:557–68.

[18] Jeong H-S, Kang S-S, Obara Y. Influence of surrounding environments and strain rates on the strength of rocks subjected to uniaxial compression. Int J Rock Mech Min Sci 2007;44(3):321–31.

[19] ISRM. Suggested methods for determining tensile strength of rock materials. Int J Rock Mech Min Sci 1978;15:99–103.

[20] ISRM. Suggested methods for determining strength of rock materials in triaxial compression: revised version. Int J Rock Mech Min Sci 1983;20:285–90.

[21] Charles RJ. Static fatigue of glass. J Appl Phys 1958;25:1549–60.

[22] ISRM SM. Suggested methods for determining the fracture toughness of rock. Int J Rock Mech Min Sci 1988;25:71–96.

[23] Backers T. Fracture toughness determination and micromechanics of rock under Mode I and Mode II loading. PhD thesis, University of Potsdam, 2005, 137pp.

[24] Backers T, Stephansson O, Rybacki E. Rock fracture toughness testing in mode II—punch-through shear test. Int J Rock Mech Min Sci 2002;39:755–69.

[25] Weibull WA. Statistical distribution function of wide applicability. J Appl Mech 1951;18:293.

[26] Golshani A, Oda M, Okui Y, Takemura T, Munkhtogoo E. Numerical simulation of the excavation damage zone around an opening in brittle rock. Int J Rock Mech Min Sci 2007;44: 835–45.

[27] Adachi T, Oka F, Koike M. An elasto-viscoplastic constitutive model with strain-softening for soft sedimentary rocks. Soils Found 2005; 45(2):125–33.

[28] Golshani A, Okui Y, Oda M, Takemura T. A micromechanical model for brittle failure of rock and its relation to crack growth observed in triaxial compression tests of granite. Mech Mater 2005; 38:287–303.

[29] Cundall PA. A discontinous future for numerical modeling in geomechanics? Geotech Eng 2001;149(1):41–7.

[30] Okubo S, Nishimatsu Y. Uniaxial compression testing using a linear combination of stress and strain as the control variable. Int J Rock Mech Min Sci 1985;22(5):323–30.

[31] Pan P-Z, Feng X-T, Hudson JA. Simulations on Class I and Class II curves by using the linear combination of stress and strain control method and elasto-plastic cellular automata. Int J Rock Mech Min Sci 2006;43(7):1109–17.
[32] Feng X-T, Pan P-Z, Zhou H. Simulation of the rock microfracturing process under uniaxial compression using an elasto-plastic cellular automaton. Int J Rock Mech Min Sci 2006;43(7):1091–108.
[33] Xu B. Plastic mechanics. Beijing: Higher Education Press; 1988 [in Chinese].
[34] Dems K, Mroz Z. Stability condition for brittle plastic structure with propagation damage surface. J Struct Mech 1985;13(1):85–122.
[35] Shen X, Cen Z, Xu B. The characteristics of elasto-brittle-plastic softening constitutive theory and its numerical calculation. J Tsinghua Univ (Sci Tech) 1995;5(2):22–7 [in Chinese].
[36] Zheng H, Liu DF, Lee CF, Ge XR. Principle of analysis of brittle-plastic rock mass. Int J Solids Struct 2005;42:139–58.
[37] Potyondy DO, Cundall PA, Lee CA. Modeling rock using bonded assemblies of circular particles. In: Aubertin M, et al., editors. Rock mechanics tools and techniques (Proceedings of the second North American rock mechanics symposium NARMS96). Rotterdam: Balkema; 1996. p. 1937–44.
[38] Potyondy DO, Cundall PA. A bonded-particle model for rock. Int J Rock Mech Min Sci 2004;41(8):1329–64.
[39] Potyondy DO. Simulating stress corrosion with a bonded-particle model for rock. Int J Rock Mech Min Sci 2007;44(5):677–91.
[40] Itasca Consulting Group. PFC^{2D} User's manual, Ver 3.0, Minneapolis, 2003.
[41] Koyama T, Jing L. Effects of model scale and particle size on micro-mechanical properties and failure processes of rocks—a particle mechanics approach. Eng Anal Bound Elem 2007;31(5):458–72.
[42] Koyama T, Jing L. Particle mechanics approach for simulating micro-structure damage and failure processes of rock core samples due to different fluid salinity. In: Proceedings of the second international conference on coupled T-H-M-C processes in geo-systems (GeoProc 2006), 2006; p. 569–74.
[43] Crouch SL. Solution of plane elasticity problems by the displacement discontinuity method. Int J Num Methods Eng 1976;10:301–43.
[44] Shen B, Rinne M, Stephansson O. FRACOD^{2D} User's manual ver 2.1, 2005, 82pp.
[45] Shen B, Stephansson O. Modification of the G-criterion of crack propagation in compression. Eng Fract Mech 1993;47(2):177–89.
[46] Staub I, Andersson JC, Magnor B. Äspö Pillar Stability Experiment, geology and mechanical properties of the rock mass in TASQ. SKB report R-04-01, Stockholm, 2004, 210pp.
[47] Hudson JA, Fairhurst C. Tensile strength, Weibull's theory and a general statistical approach to rock failure. In: Te'eni M, editor. Proceedings of the international conference on structure, solid mechanics & engineering design in civil engineering materials, Part II. 1969; p. 901–14.
[48] Lemaitre J. A course on damage mechanics. Berlin: Springer; 1992.